

Design and test for muon detectors based on extruded scintillator and SiPM

Hongyu Zhang,¹ Xiyang Wang,¹ Weihu Ma,¹ Shiming Zou,¹ Deqing Fang,¹ Wanbing He,^{1,2} Xiaolong Wang,^{1,*} Zhen Wang,^{3,4,5} Rui Yuan,^{3,4,5} and Qibin Zheng⁶

¹*Key Laboratory of Nuclear Physics and Ion-beam Application (MOE) and Institute of Modern Physics, Fudan University, 220 Handan Road, Shanghai, 200433, China*

²*Shanghai Research Center for Theoretical Nuclear Physics, NSFC and Fudan University, Shanghai, 200438, China*

³*Tsung-Tao Lee Institute, Shanghai Jiao Tong University, 520 Shengrong Road, Shanghai 201210, China*

⁴*Institute of Nuclear and Particle Physics, School of Physics and Astronomy, 800 Dongchuan Road, Shanghai 200240, China*

⁵*Key Laboratory for Particle Astrophysics and Cosmology (MOE), Shanghai Key Laboratory for Particle Physics and Cosmology (SKLPPC), Shanghai Jiao Tong University, 800 Dongchuan Road, Shanghai 200240, China*

⁶*Laboratory of Radiation Detection and Medical Imaging and School of Health Science and Engineering, University of Shanghai for Science and Technology, Shanghai, 200093, China*

A combination of scintillator, wavelength shifting (WLS) fiber, and silicon photomultiplier (SiPM) shows an excellent performance in the ‘ K_L and μ detector (KLM)’ of the Belle II experiment. We describe the R&D for a similar detection technology with a new scintillator and SiPM, which can be implemented for a muon detector for the proposed CEPC experiment and the upgrade of KLM in Belle II. The R&D contains the study of the performance of a new scintillator with a length of 150 cm, the NDL SiPM with a sensitive surface of $3\text{ mm} \times 3\text{ mm}$ or the Hamamatsu MPPC with a sensitive surface of $1.3\text{ mm} \times 1.3\text{ mm}$, the construction of a detector strip, and the methods to achieve excellent light collection. The cosmic ray tests show good photon collections by NDL SiPM or MPPC, efficiencies well above 90% with a threshold of 8 *p.e.*, and time resolutions of better than 1.7 ns for the hits at the far end of a scintillator strip. The performance shows a good option for an excellent muon detector for CEPC and the possible upgrade of Belle II KLM.

Keywords: Muon detector, scintillator, silicon photomultiplier, CEPC

I. INTRODUCTION

In the Standard Model of particle physics, the Higgs boson (H) plays a fundamental role in elucidating the origin of matter mass. The mass of $m_H \approx 125 \text{ GeV}/c^2$ makes it possible for a new e^+e^- collider running at the center-of-mass energy $\sqrt{s} \sim 240 \text{ GeV}$ as a Higgs factory. The dominant mechanism for Higgs boson production in e^+e^- annihilation is $e^+e^- \rightarrow H + Z^0$, where Z^0 is the gauge boson for neutral weak interaction with branching fraction of decays $\mathcal{B}(Z^0 \rightarrow \mu^+\mu^-) = (3.3662 \pm 0.0066)\%$ [1]. In many measurements, the H boson can be determined well in the recoil of the Z^0 boson, which can be reconstructed well in its $\mu^+\mu^-$ decay mode. This requires an excellent measurement of the muons. There have been proposals, such as the International Linear Collider [2, 3], the Circular Electron Positron Collider (CEPC) [4, 5], and the Future Circular Collider [6]. The proposal of CEPC started in 2013, followed by comprehensive R&D for the accelerator and the detector.

As discussed in the Conceptual Design Report of CEPC, the muon detector is the system that can identify muons, detect leakage of showers from the calorimeters, and search for a long-lived particle [5]. To provide more information on the physics processes involving muon final states, the muon system should perform well in terms of detection efficiency, low hadron misidentification rate, proper position resolution, and extensive coverage. Furthermore, the clean muon hits in the muon detector are an excellent input for the trigger system.

The ' K_L and μ detector (KLM)' of the Belle II experiment [7] shows a good reference for a muon detector in the CEPC experiment. As the upgrade of the Belle experiment [8], the Belle II experiment [7] is a super B factory, aiming at a luminosity of $0.65 \times 10^{36} \text{ cm}^{-2}\text{s}^{-1}$ to collect a data sample of 50 ab^{-1} e^+e^- collision events. The Resistive Plate Chambers (RPCs) for KLM in Belle are partially replaced in Belle II by scintillator modules made of plastic scintillator strips, wave-length-shift (WLS) fiber, silicon photomultiplier (SiPM), and these scintillator modules are working well [9]. Soon after the physics run in 2019 started, an Upgrade Working Group was formed in the Belle II Collaboration to perform the R&D for the upgrade of Belle II in the future [10, 11]. The proposal for the KLM upgrade contains replacing 13 barrel layers of legacy RPCs with scintillators, on-detector upgraded scintillator readout, and high precision timing for K_L momentum measurement.

In this article, we introduce the R&D for a new detector that can be used for CEPC muon detector and Belle II KLM upgrade based on extruded plastic scintillator, WLS fiber, and SiPM. We focus the R&D on the scintillator strips and SiPMs being made in China and WLS fiber from Kuraray Company.

* Corresponding author, xiaolong@fudan.edu.cn

We show how to achieve a good photon collection by improving the couplings among the scintillator strip, the WLS fiber, and the SiPM. We also study the time resolution of this design, which could help in developing triggers from the muon detector and suppress the backgrounds by shortening the time window of hit signals, which could be used to improve the identification of muon or neutral hadron-like K_L . The R&D also shows a good option for the muon detector of Super Tau-Charm Facility [12] and a hadronic calorimeter for the DarkSHINE experiment [13].

II. BELLE II KLM AND THE SCHEME OF A DETECTOR CHANNEL

As the outermost system of the Belle II detector, KLM identifies K_L and muons with momenta up to 4.5 GeV/ c . As shown in Fig. 1(a), KLM spans radii of 200 – 240 cm in the octagonal barrel and 130 – 340 cm in the forward and backward endcaps. The barrel section comprises 15 detector layers and 14 yoke iron layers, while each endcap consists of 14 detector layers and 14 iron layers. The yoke layer plays a dual role, serving as a magnetic flux reflow for the solenoid and an enabler for hadron cascade clustering in K_L . Large-surface-area detector panels of about 3.1 cm thickness are sandwiched in the gaps between the steel plates of 4.7 cm thickness. In the panels, the innermost two layers of the barrel and all the layers of the endcaps contain scintillator strips, and the remaining 13 layers of the barrel contain the legacy RPCs from the Belle experiment. Each detector panel provides two orthogonal measurements of a through-going particle's position via hits on these strips. There are about 38,000 readout channels in the KLM, of which half are for the scintillators.

In the scintillator modules, the cross section of each barrel (endcap) scintillator strip is 4 cm \times 1 cm (4 cm \times 0.75 cm). An embedded Kuraray Y11(200)MSJ WLS fiber [14] collects photons from each scintillator strip and detected by a SiPM, also known as a Multi-Pixel Photon Counter (MPPC: Hamamatsu S10362-13-050C). An MPPC is affixed directly to the scintillator strip at one end of the WLS fiber. The signals are preamplified internally by a factor of ~ 10 and then routed via ribbon cables to external readout electronics mounted on the magnet yoke. Figure 1(b) shows the internal of a scintillator module built at Virginia Tech for the barrel KLM in 2013. Details about the R&D for Belle II endcap KLM are described in Ref. [15]. Figure 1(c) shows a spare KLM module we got from KEK to reference this R&D work. The spare KLM module shows a compact and simple design for the detection based on the scintillator.

We use a design similar to the Belle II KLM for a detector channel based on an extruded scintillator, as shown in Fig. 2. The structure of the detector channel contains a long scintillator strip with a geometry of 1 cm \times 4 cm \times 150 cm, a WLS fiber inside the strip, a SiPM on a small printed circuit board (PCB), and

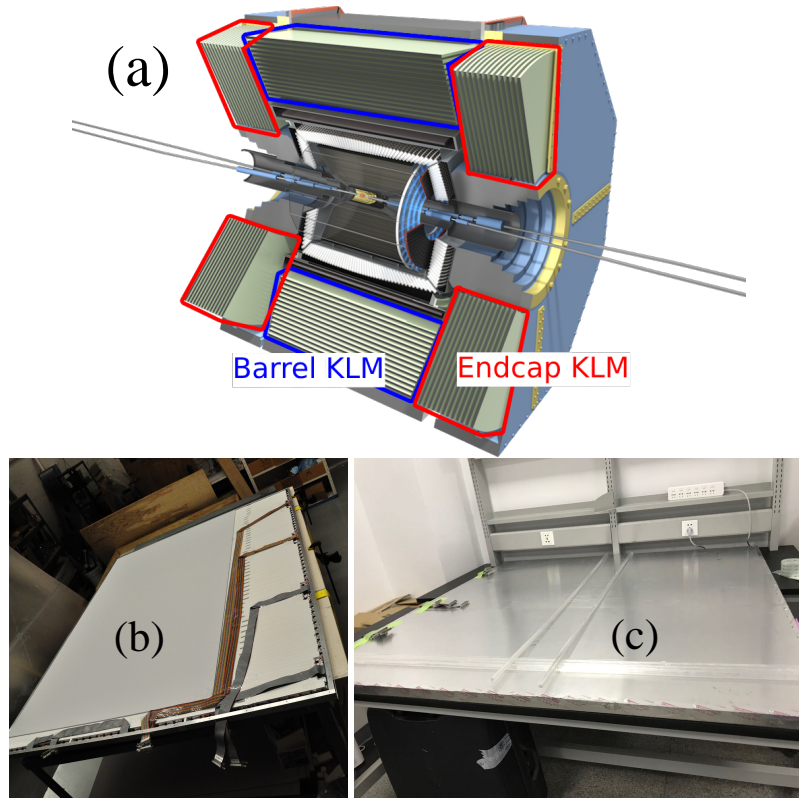


Fig. 1. The KLM system in the Belle II detector and a scintillator module for the barrel KLM.

a coupling component to mount the fiber to the SiPM.

III. THE MAJOR COMPONENTS FOR A DETECTOR CHANNEL

A detector channel has four major components: scintillator strip, WLS fiber, SiPM [16], and electronic readout containing preamplifier [17–19]. For these components, we designed the readout [20], got scintillator strips and SiPMs made by companies in Beijing, and purchased the same WLS fiber from Kuraray. In this way, we can save the cost of a possible massive production of scintillator modules for a large muon detector.

A. Scintillator and WLS fiber

Remarkable performance has been achieved with scintillator strips from established producers such as Fermilab and Uniplast for the current Belle II KLM [7]. The scintillator strips used in this R&D work are manufactured by the GaoNengKeDi company [21] using polyethylene and extrusion technique [22]. The

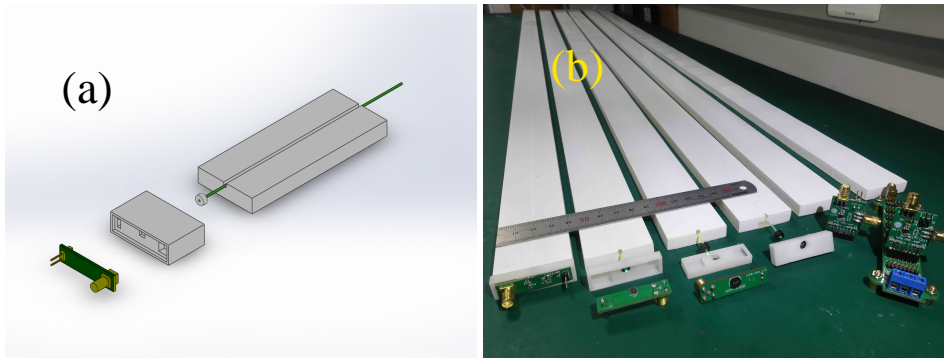


Fig. 2. The structure of a detector channel, which contains a long scintillator strip with a geometry of $150\text{ cm} \times 4\text{ cm} \times 1\text{ cm}$, a WLS fiber inside the strip, a SiPM on a small PCB with a preamplifier, connectors to hold the fiber and mount it to the SiPM.

attenuation length of such a scintillator is only several centimeters, while a WLS fiber has an attenuation length of several meters. Embedding a WLS fiber in the scintillator [23] can obtain a sufficiently high light collection, which helps to keep an excellent detection efficiency at a large length. A long groove with a width of about 2 mm and a depth of about 4 mm is embedded in the scintillator to lay a WLS fiber. We try the BCF-92 fiber from Saint-Gobain [24, 25] and the Y11(200) from Kuraray [14]. The diameters of Kuraray fiber and Saint-Gobain fiber are 1.2 mm and 1.0 mm, respectively. The light yield performance of two kinds of WLS fiber is measured by comparing the fired pixels of SiPM. The tests show that the light yield achieved with Kuraray fiber is typically 2.3 times that obtained with Saint-Gobain fiber.

The Y11(200) is a blue-to-green shifter with diameter of 1.2 mm and a emission spectrum peaking at 476 nm [14]. From the datasheet, the attenuation length of Y11(200) is $> 3.5\text{ m}$. By measuring the light yield of the scintillator with WLS fiber at various positions, we determine the effective attenuation length using a fitting function comprising two exponential decay functions. The effective attenuation length consists of a long attenuation length $L_l \approx 2.63\text{ m}$ and a short attenuation length $L_s \approx 6\text{ cm}$.

B. Hamamatsu MPPCs and NDL SiPMs

A SiPM comprises a high-density matrix of avalanche photodiodes operating in Geiger mode and is distinguished by its high photon detection efficiency, high gain, excellent time resolution, low operation voltage, ruggedness, and magnetic field resistance. Typically, the quantum efficiency is close to 50%. When photons arrive at a SiPM, pixels are fired via the Photoelectric Effect, and electrons are generated and amplified. There are thermally induced electrons, even without light input. This is called dark count-

ing. An electron generated and amplified in a SiPM is called a photo-electron ($p.e.$), whether from a signal or a dark counting background. The output pulse height varies proportionately to the number of photoelectrons ($N_{p.e.}$), which can be distinguished in the ADC distribution of signals from a SiPM.

We employ two types of SiPMs: the S13360 series MPPC manufactured by Hamamatsu company [26] and the EQR15 11-3030D-S series SiPM from the Novel Device Laboratory (NDL) [27, 28]. Compared to the S10362 series utilized in the current KLM, the S13360 series of MPPC have the same $1.3 \text{ mm} \times 1.3 \text{ mm}$ sensitive area, while lower operation voltages and reduced cross-talk and dark counting rates (DCR). The smallest NDL SiPM is the EQR10 11-1010-C-S series with a sensitive area of $1.0 \text{ mm} \times 1.0 \text{ mm}$, which is smaller than the Y11 WLS fiber. Instead, we use the EQR15 11-3030D-S series with a sensitive area of $3.0 \text{ mm} \times 3.0 \text{ mm}$.

We study the characteristics of Hamamatsu MPPCs and NDL SiPMs before their implementation in the setup. These characteristics are the breakdown voltage, the gain, the DCR, and the cross-talks, which are shown in Fig. 3. The breakdown voltage of a diode is the reversed bias voltage that SiPM starts to work when the avalanche breakdown begins. The standard procedure is to measure the current with the reversed bias voltage. The gain of a SiPM is defined as the charge collected by the SiPM for a single $p.e.$ signal (SPE) [29]. The experimental tests yield the gains of 4.6×10^5 for the S13360 MPPC operating at 57.0 V and 2.9×10^5 for the EQR15 11-3030D-S operating at 27 V. The gain of EQR15 11-3030D-S has a good agreement to the datasheet from NDL [27].

The dark counting is a rollback in using SiPM for photon detection, especially in SPE detection. The rate of dark counting (DCR) of a SiPM is evaluated by processing the raw waveforms and counting the number of dark pulses that exceed some fixed $N_{p.e.}$ threshold. Here, we take the threshold of SPE. A photon that produces an avalanche inside a pixel can generate another in the neighboring pixels. This phenomenon is called the optical cross-talk, defined as the DCR ratio for pulses exceeding the $1.5 p.e.$ and $0.5 p.e.$ levels. As shown in Fig. 3, Hamamatsu MPPC has a one-order lower DCR than NDL SiPM, and the cross-talk of NDL SiPM increases fast along with the overvoltage. It should be mentioned that the pixel size of MPPC S13360 is $50 \mu\text{m}$, and the one of NDL EQR15 11-3030D-S is $15 \mu\text{m}$.

C. Readout electronics and data acquisition system

Generally, the operation of a SiPM requires a signal amplification circuit and an external power supply [30, 31]. We developed a new preamplifier with a gain of 21 and adopted the form of negative feedback to improve gain stability [20]. The preamplifier has a time resolution better than 50 ps. The power supply

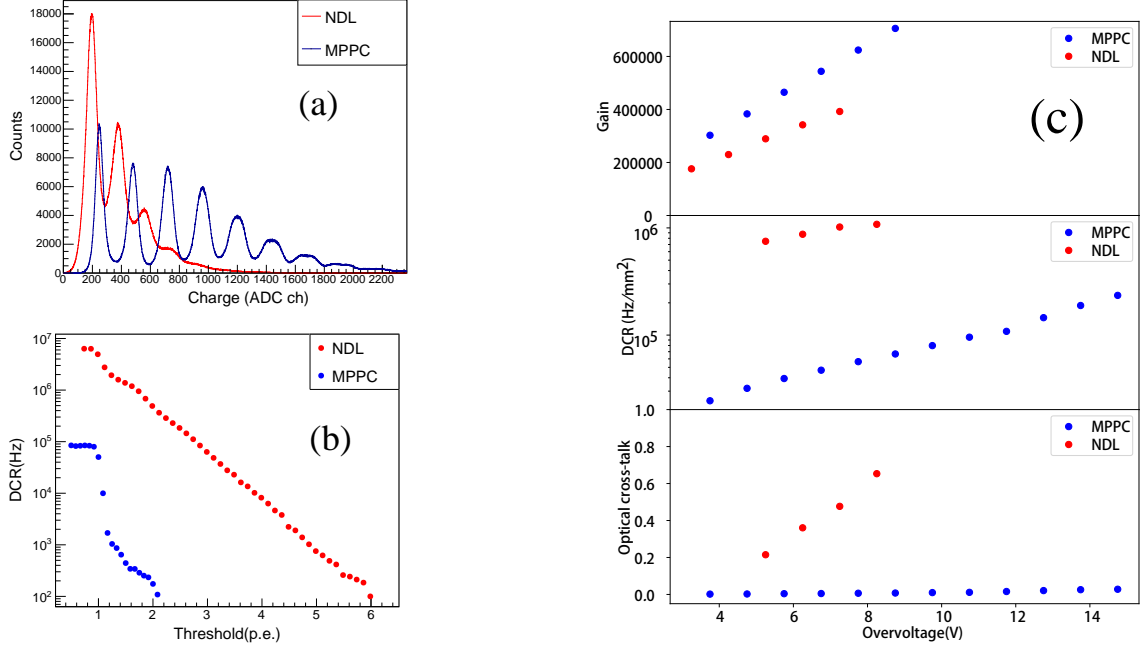


Fig. 3. Characteristics of SiPMs used in the R&D. The plot (a) shows the photon spectra of Hamamatsu MPPC operating at $HV = 56.0$ V and NDL SiPM operating at $HV = 27.0$ V, where up to 8 $p.e.$ peaks and 4 $p.e.$ peaks are visible in signals from MPPC and NDL SiPM, respectively. Plot (b) shows the dark counting rates of MPPC and NDL SiPM versus the thresholds of $N_{p.e.}$. Plot (c) shows the variations of the gain, the dark counting rate, and the optical cross-talk with the overvoltage of MPPC and NDL SiPM.

motherboard has a voltage regulator module that supplies both high voltage for SiPM operation and low voltage for the preamplifier.

We use a high-sampling-rate Tektronix MSO58 oscilloscope or an MDO3024 oscilloscope controlled by a PC and configured with trigger logic to store the waveform data of the signals [32]. We obtain detailed information on ADC, TDC, baseline, timing, etc. [33, 34], from the offline analysis of the waveforms. In this way, we set up the tests for a long time of data taking and then investigate the signals and the possible backgrounds in the offline data analyses. For example, we study the pulse heights or the ADC for the $N_{p.e.}$ and obtain the time information from the waveforms by discriminating the leading edge or using the constant fraction discrimination method.

IV. IMPROVEMENTS FOR THE PHOTON COLLECTION

During the R&D, we find that the couplings among fiber, scintillator, and SiPM for an excellent light collection are essential for the performance of the detector channel [35], such as the detection efficiency and the time resolution. We design a coupling component to hold WLS fiber and SiPM, polish the surface of the WLS fiber terminal, coat the scintillator with a reflection layer, and use optical glue in the scintillator groove. To study the performance, we trigger the cosmic rays passing through the long strip at different positions. We measure the pulse height of a SiPM signal and then convert it to $N_{p.e.}$. The $N_{p.e.}$ obtained from the SiPM signals in the tests obey the Landau distributions well, so we employ Landau functions to fit the $N_{p.e.}$ distributions. Figure 4 shows the resulting means, denoting the number of fired pixels, along with standard deviations represented by error bars.

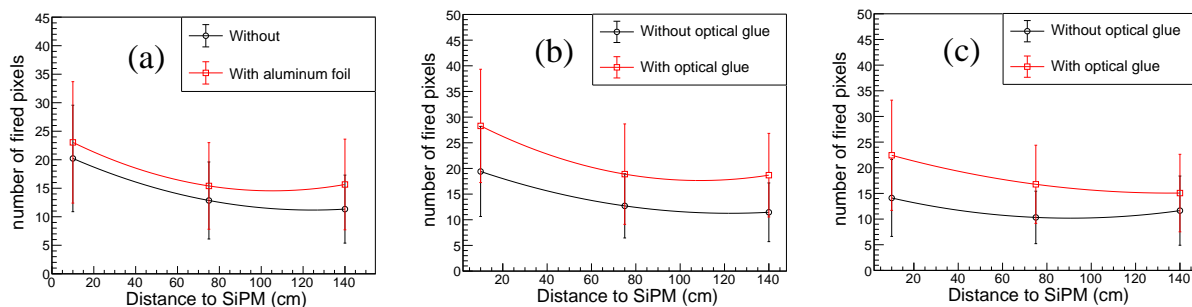


Fig. 4. Distribution of the average $N_{p.e.}$ as a function of the distance from a hit on the scintillator strip to the SiPM. Plot (a) is the comparison between with and without aluminum foil, and (b) with TiO_2 and (c) with Teflon are comparisons between with and without using optical glue. The dots and the error bars are the means and the standard deviations from fitting to the $N_{p.e.}$ distributions with Landau functions.

The coupling component used in the Belle II experiment is improved in our R&D to simplify the detection system assembly and improve the photon detection. As shown in Fig. 2, this component yields excellent stability of the connection between the terminal surface of WLS fiber and the sensitive area of SiPM. We produce these components with a 3D printer.

We polish the terminal surface of the fiber with sandpaper and find that 2000 mesh is good enough for a relatively flat surface. This is helpful in using the MPPC S13360 with a sensitive area of $1.3 \text{ mm} \times 1.3 \text{ mm}$. In Belle II, it was found that the closeness between fiber and SiPM affects about 37% in photon collection, mainly due to the diffuse transmission at the fiber terminal surface. NDL EQR15 11-3030D-S has a large sensitive area of $3.0 \text{ cm} \times 3.0 \text{ cm}$, about five times that of MPPC S13360. We find that polishing

the terminal surface of the fiber well is unnecessary to improve the photon collection when using NDL EQR15 11-3030D-S.

We coat the scintillator strips with reflective layers and then use black plastic tapes to shield ambient light and stop cross-talk between strips. We also compare strips with and without aluminum foil and find that using aluminum foil can increase the $N_{p.e.}$ by 38% at the far end, as shown in Fig. 4(a). A comparative test with the reflective layers demonstrates that TiO_2 performs slightly better than Teflon, as shown in Fig. 4(b) and (c). However, Teflon coating offers the advantages of ease of production and lower cost. Therefore, we propose considering the utilization of a thicker Teflon coating in the study to optimize the performance further.

We use optical glue to enhance the coupling between the fiber and the scintillator. In a test involving TiO_2 -coated strips, the application of optical glue yields a substantial increase of 63% in $N_{p.e.}$ at the far end of the strips, as shown in Fig.4(b). Additionally, Teflon-coated strips exhibited a 30% improvement, as shown in Fig.4(c).

V. PERFORMANCE OF AN ARRAY OF SCINTILLATOR STRIPS IN COSMIC RAY TESTS

Like the KLM of Belle II shown in Fig. 1, a muon detector typically has several layers of detector modules for charged track [36] detection [7]. According to the experience with KLM, the key to the R&D of a muon detector based on extruded scintillator is to have good efficiencies simultaneously from scintillator strips. We put six detector channels together as an array and study the performance of this array in tests with cosmic rays, as shown in Fig. 5(a). We use two short strips with a length of 10 cm as triggers [37] aligned vertically at the top and the bottom of the six long strips. The optimized operation voltages for the MPPC S13360 and the NDL EQR15 11-3030D-S are 56 V and 27 V, respectively, according to the performances shown in Fig. 3. The amplitude of the SPE signal is about 2 mV. The typical signal waveforms from two triggers and six strips are shown in Fig. 5(b).

Like the study shown in Fig. 4, we measure the ADC distributions of the array at different positions and then convert them to the distributions of $N_{p.e.}$. We fit the $N_{p.e.}$ distributions with Landau functions again and show the means and the standard deviations of the Landau functions in Fig. 6(a1) and (a2). The six strips with NDL SiPMs show similar performance in photon collection; up to 34 $p.e.s$ per cosmic ray are observed at the near end, and 23 $p.e.s$ at the far end with aluminum foil used to enhance the reflection layer. Considering the different cross-talks, NDL SiPMs and Hamamatsu MPPCs perform similarly in photon collection. No noticeable reduction of $N_{p.e.}$ with a distance larger than 75 cm indicates that the

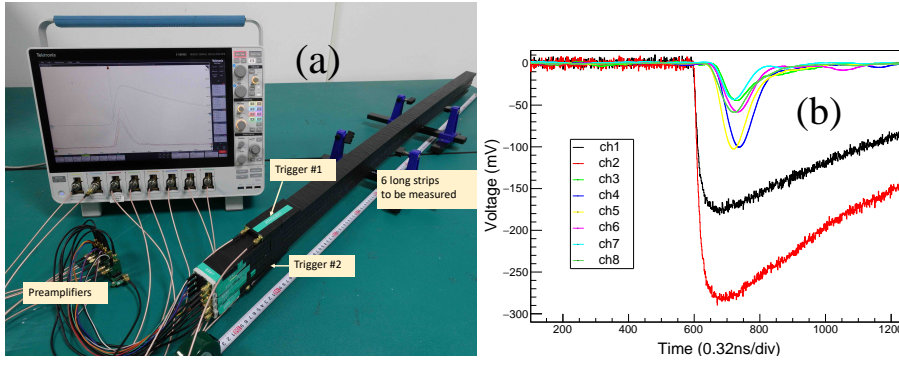


Fig. 5. Setup for cosmic ray test of six long strips including preamplifiers and oscilloscope, and the waveform fetched by the oscilloscope of six channels and two trigger channels at the far end. The ch1 and ch2 in plot (b) are the Trigger#1 and Trigger#2 in plot (a), and ch3-ch8 are the six long strips.

long attenuation length of the WLS fiber is beneficial for excellent detection efficiency in a long scintillator strip.

The efficiency performance at the far end was assessed using the six strips with MPPCs and NDLSiPMs, respectively. As shown in Fig. 6(b1) and (b2), the efficiency of the majority of strips using NDLSiPM is higher than 90% at a threshold of 10.5 $p.e.s$. Similarly, for strips equipped with MPPCs, the efficiency surpasses 84% at the same threshold level. These results demonstrate the favorable efficiency of NDLSiPM and MPPC SiPMs for detecting events at the far end of the strips. It should be mentioned that there are some differences among the six strips due to the assembling quality of SiPM and fiber.

Regarding the measured results at the operation voltages, the optical cross-talk of NDLEQR15 11-3030D-S is about 20%, whereas the one of MPPC S13360 is about 1%. To study the performance of the arrays, we compare the number of responded strips at a threshold of 9.5 $p.e.s$ for NDLSiPM and 7.5 $p.e.s$ for MPPC. As shown in Fig. 6(e1) and (e2), approximately 90% of cosmic rays result in a signal response for all MPPC strips. This ratio is about 70% in the test with NDLSiPMs. In the requirement of at least five strips having hits, the efficiency of cosmic ray detection is about 95% when using NDLSiPMs and about 99% when using Hamamatsu MPPCs. Therefore, we can expect very high efficiency of a robust and compact muon detector built with several layers of scintillators, WLS fibers, and SiPMs. For reference, the threshold of a hit signal from a scintillator channel is 8 $p.e.s$ in the current Belle II KLM.

A critical advantage of a muon detector built with scintillators is the excellent time resolution. The time resolution of KLM built with RPCs was not considered in Belle. With the time calibration, which started from the Belle II Fudan group, the KLM currently has a time resolution of about 4 ns in the endcaps

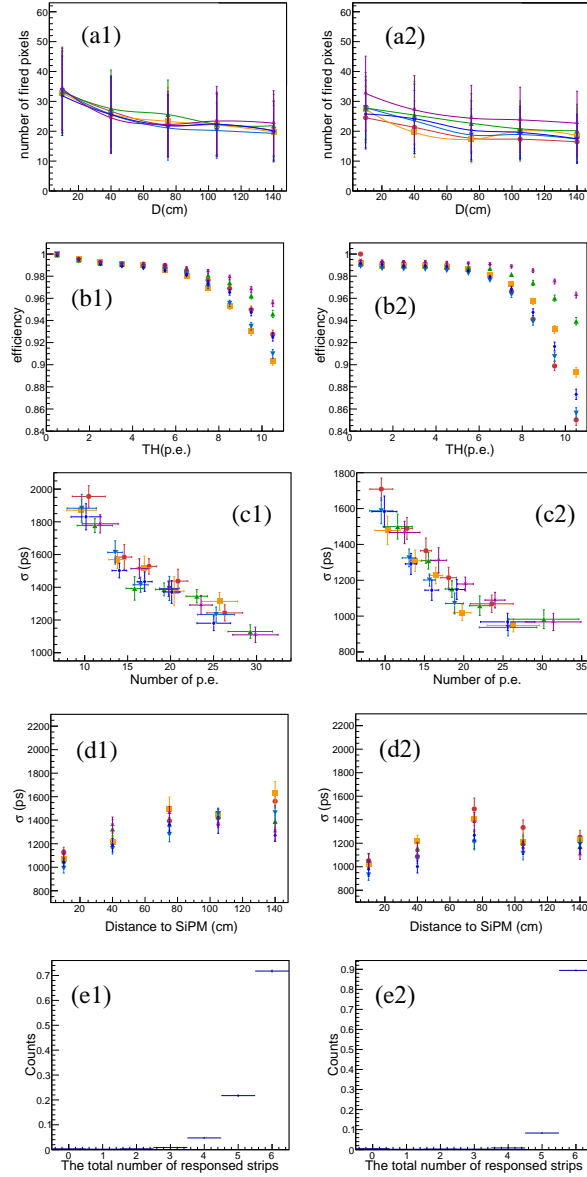


Fig. 6. The performance of the setups of detector arrays in cosmic ray tests. The left panel is setup based on NDLSiPMs and the right one based on Hamamatsu MPPCs. Each setup has six detector channels. Plots (a1) and (a2) are the distributions of $N_{p.e.}$ from the cosmic ray hits along the strips, where the dots and the error bars are the means and the standard deviations from fitting to the $N_{p.e.}$ distributions with Landau functions. Plots (b1) and (b2) are the efficiency versus the $N_{p.e.}$ threshold at the far end. Plots (c1) and (c2) are the time resolutions versus the $N_{p.e.}$ at far end. Plots (d1) and (d2) are the time resolutions triggering at the far ends of the strips. Plots (e1) and (e2) are the distributions of the number of detector channels responding to cosmic ray tracks.

and about 8 ns in the barrel. This work is ongoing in Belle II. The basis of the performance is the time resolution that can be achieved in a detector channel. We study the time resolution of our detector channels in tests with cosmic rays [38]. The scintillator of the two trigger strips has long attenuation, and four large SiPMs are mounted to each terminal surface of one strip. We obtain a time resolution of about 60 ps from this trigger system. We lay the triggers at different positions along the long scintillator strip and measure the time difference between the signal from this detector channel and the signals from the triggers. We then calculate the time resolutions of the long the scintillator strips according to the time differences. We show the results from tests with MPPC S13360 and NDL EQR15 11-3030D-S in Fig. 6(c1) and (c2). The time resolution at the far end of a long strip is strongly related to $N_{p.e.}$. A time resolution better than 1 ns is achieved with $N_{p.e.} > 35$ using NDL EQR15 11-3030D-S and $N_{p.e.} > 30$ using MPPC S13360. A good time resolution with a large $N_{p.e.}$ can be achieved by increasing the light yield of the scintillator strip or using multiple fibers and large-size SiPM in a detector channel.

Figure 6(d1) and (d2) also display the time resolutions at various positions along the long strips, which are about 1.4 ns for NDL SiPM and about 1.2 ns for MPPC. By employing a linear fit to the signal time difference between the long strip detector and the trigger detector at several trigger positions, we obtained the velocity of scintillation photon propagation in the Kuraray fiber to be (16.3 ± 2.8) cm/ns. A test with a longer scintillator bar and fiber can improve the velocity resolution.

VI. SUMMARY

For the design of a muon detector for CEPC based on scintillator and the possible upgrade of Belle II KLM, we perform the R&D on detector technology based on extruded plastic scintillator, WLS fiber, and SiPM. Besides the preamplifier that has been designed, we use the scintillators from GNKD company, SiPMs from Hamamatsu company and NDL, and WLS fiber from Kuraray company. We study the performances of the SiPMs and increase the photon collection by designing a coupling component to hold the WLS fiber and mount it to SiPM and increasing the couplings among the scintillator, the WLS fiber, and the SiPM. We test the reflection layers with TiO_2 and Teflon and find that Teflon performs well enough. The long scintillator strips show good efficiencies higher than 90% and time resolutions better than 2 ns. The study shows that this technology can be used to build a muon detector for CEPC and upgrade Belle II KLM by replacing the legacy RPC modules.

ACKNOWLEDGMENT

This work is partially supported by the National Key R&D Program of China under Contract No. 2022YFA1601903; National Natural Science Foundation of China under Contracts No. 11925502, No. 11961141003, and No. 12175041; and the Strategic Priority Research Program of the CAS under Contract No. XDB34030000.

- [1] R.L. Workman *et al.* (Particle Data Group), The Review of Particle Physics (2023), Prog. Theor. Exp. Phys. **2022** (2022) 083C01 and 2023 update. doi:10.1093/ptep/ptac097
- [2] C. Adolphsen, M. Barone, B. Barish *et al.*, The International Linear Collider Technical Design Report - Volume 3.II: Accelerator Baseline Design, arXiv:1306.6328. doi:10.48550/arXiv.1306.6328
- [3] T. Behnke, J. E. Brau, P.N. Burrows *et al.*, The International Linear Collider Technical Design Report - Volume 4: Detectors, arXiv:1306.6329. doi:10.48550/arXiv.1306.6329
- [4] The CEPC Study Group, CEPC Conceptual Design Report: Volume 1 - Accelerator. arXiv:1809.00285v1. doi:10.48550/arXiv.1809.00285.
- [5] The CEPC Study Group, CEPC Conceptual Design Report: Volume 2 - Physics & Detector. arXiv:1811.10545v1. doi:10.48550/arXiv.1809.00285.
- [6] The FCC Collaboration, FCC Physics Opportunities. Eur. Phys. J. C **79** (2019) 474. doi:10.1140/epjc/s10052-019-6904-3
- [7] T. Abe, I. Adachi, K. Adamczyk *et al.*, The Belle II Technical Design Report, KEK Report 2010-1, 2010, arXiv:1011.0352v1. doi:10.48550/arXiv.1011.0352.
- [8] A. Abashian, K. Gotow, N. Morgan *et al.* (Belle Collaboration), The Belle detector. Nucl. Instrum. Methods A **479** (2002) 117. doi:10.1016/S0168-9002(01)02013-7.
- [9] LeptonID group and Belle II Collaboration, Muon and electron identification efficiencies and hadron-lepton misidentification rates at Belle II for Moriond 2021, Mar 2021. BELLE2-CONF-PH-2021-002.
- [10] P. Križan *et al.* (Belle II Collaboration), The Belle II Upgrade Program. arXiv:2211.13634. doi:10.48550/arXiv.2211.13634
- [11] F. Forti (for the Belle II Collaboration), Snowmass Whitepaper: The Belle II Detector Upgrade Program. arXiv:2203.11349v1. doi:10.48550/arXiv.2203.11349.

- [12] M. Achasov *et al.*, STCF conceptual design report (Volume 1): Physics & detector. *Front. Phys.* **19**(1) (2024) 14701. doi:10.1007/s11467-023-1333-z
- [13] J. Chen *et al.*, Prospective study of light dark matter search with a newly proposed DarkSHINE experiment. *Sci. China-Phys. Mech. Astron.* **66**(1) (2023) 211062. doi:10.1007/s11433-022-1983-8
- [14] Kuraray, Ltd. (Japan), <https://www.kuraray.com/products/psf>[Accessed 20 Nov 2023]
- [15] T. Aushev, D.Z. Besson, K. Chilikin *et al.*, A scintillator based endcap K and muon detector for the Belle II experiment. *Nucl. Instrum. Methods A* **789** (2015) 134. doi:10.1016/j.nima.2015.03.060
- [16] Q.Y. Wei, T.P. Xu, T.T. Dai *et al.*, Development of a compact DOI-TOF detector module for high-performance PET systems. *Nucl. Sci. Tech.* **28** (2017) 43. doi:10.1007/S41365-021-00965-0.
- [17] Y. Yang, P.C. Yang, J.Xin *et al.*, Performance of a plastic scintillation fiber dosimeter based on different photoelectric devices. *Nucl. Sci. Tech.* **32** (2021) 120. doi:10.1007/S41365-021-00965-0.
- [18] M. Li, Z.M. Wang, C.M. Liu *et al.*, Performance of compact plastic scintillator strips with wavelength shifting fibers using a photomultiplier tube or silicon photomultiplier readout. *Nucl. Sci. Tech.* **34** (2023) 31. doi:10.1007/s41365-023-01175-6.
- [19] J.Y. Chen, J.F. Tong, Z.L. Hu *et al.*, Evaluation of neutron beam characteristics for D-BNCT01 facility. *Nucl. Sci. Tech.* **33** (2022) 12. doi:10.1007/s41365-022-00996-1
- [20] X.Y. Wang, H.Y. Zhang, D.Q. Fang *et al.*, Design and performance of a high-speed and low-noise preamplifier for SiPM. *Nucl. Sci. Tech.* **34** (2023) 169. doi:10.1007/s41365-023-01328-7
- [21] BEIJING GAONENG KEDI TECHNOLOGY CO. Ltd. (China), <http://www.gaonengkedi.com/>[Accessed 20 Nov 2023]
- [22] J. W. Seo, E.J. Jeon, W.T. Kim *et al.*, A feasibility study of extruded plastic scintillator embedding WLS fiber for AMoRE-II muon veto. *Nucl. Instrum. Methods A* **1039** (2022) 167123. doi:10.1016/j.nima.2022.167123
- [23] G. Luo, Y.K. Hor, P.Z. Lu *et al.*, Design optimization of plastic scintillators with wavelength-shifting fibers and silicon photomultiplier readouts in the top veto tracker of the JUNO-TAO experiment. *Nucl. Sci. Tech.* **34** (2023) 99. doi:10.1007/s41365-023-01263-7.
- [24] Saint-Gobain, Ltd. (France), <https://www.crystals.saint-gobain.com/radiation-detection-scintillators/fibers>[Accessed 20 Nov 2023]
- [25] J.N. Dong, Y.L. Zhang, Z.Y. Zhang *et al.*, Position-sensitive plastic scintillator detector with WLS-fiber readout. *Nucl. Sci. Tech.* **29** (2018) 117. doi:10.1007/s41365-018-0449-2.
- [26] Hamamatsu Photonics K.K. (Japan), https://www.hamamatsu.com/eu/en/product/optical-sensors/mppc/mppc_mppc-array.html[Accessed 20 Nov 2023]

- [27] Novel Device Laboratory (China), <http://www.ndl-sipm.net/> [Accessed 20 Nov 2023]
- [28] J.Q. Jia, J.L. Jiang, K. Liang *et al.*, EQR SiPM with P-on-N diode configuration. Nucl. Sci. Tech. **30** (2019) 119. doi:10.1007/s41365-019-0644-9.
- [29] W. Wang, X.X. Yuan, X.H. Cai, A beam range monitor based on scintillator and multi-pixel photon counter arrays for heavy ions therapy. Nucl. Sci. Tech. **33** (2022) 123. doi:10.1007/s41365-022-01113-y.
- [30] Y.Y. Li, C.Y. Li, K. Hu, Design and development of multi-channel front end electronics based on dual-polarity charge-to-digital converter for SiPM detector applications. Nucl. Sci. Tech. **34** (2023) 18. doi:10.1007/s41365-023-01168-5
- [31] H. Wang, D. Wang, R. Chen *et al.*, Electronics system for the cosmic X-ray polarization detector. Nucl. Sci. Tech. **34** (2023) 64. doi:10.1007/s41365-023-01221-3
- [32] K. Wang, S. Samaranayake, A. Estrade, Investigation of a digitizer for the plastic scintillation detectors of time-of-flight mass measurements. Nucl. Instrum. Methods A **1027** (2022) 166050. doi:10.1016/j.nima.2021.166050.
- [33] R.S. Dong, L. Zhao, J.J. Qin *et al.*, Design of a 20-Gsps 12-bit time-interleaved analog-to-digital conversion system. Nucl. Sci. Tech. **32** (2021) 25. doi:10.1007/s41365-021-00863-5
- [34] H.K. Wu, C. Li, A ROOT-based detector test system. Nucl. Sci. Tech. **32** (2021) 115. doi:10.1007/s41365-021-00952-5
- [35] L. Ding, Q. Wu, Q. Wang *et al.*, Advances on inorganic scintillator-based optic fiber dosimeters. Nucl. Sci. Tech. **7** (2020) 60. doi:10.1186/s40658-020-00327-6
- [36] K. Zhang, M. He, W. Li *et al.*, Muon tracking with the fastest light in the JUNO central detector. Radiat Detect Technol Methods **2** (2018) 13. doi:10.1007/s41605-018-0040-8
- [37] S. Wang, W. Chen, J.H. Guo, Design and testing of a miniature silicon strip detector. Nucl. Sci. Tech. **31** (2020) 7. doi:10.1007/s41365-019-0714-z
- [38] S.L. Li, Y.K. Heng, T. C. Zhao *et al.*, Method for improving the time resolution of a TOF system. Chin. Phys. C **37** (2013) 016003. doi:10.1088/1674-1137/37/1/016003